Analysis and evaluation of drop point for water jet based on wave model

Yang Qu*, Xintian Liu*, Minghui Zhang*, Yansong Wang* and Changhong Liu**

*School of Mechanical and Automotive Engineering, Shanghai University of Engineering Science, Shanghai, China
**School of Mechanical and Power Engineering, East China University of Science and Technology, Shanghai, China
Corresponding Author: xintianster@gmail.com

ABSTRACT

To study the precision of the fire water monitor with important influence on fire extinguishing effect, the drop point of fire water monitor is studied. The quadratic drag model is selected on the basis of the analysis of the mechanical model of the fluidic microbody, considering the change of the cross-sectional area caused by velocity and breakup of the water jet. The boundary between breakup and atomization is clarified, and the change of diameter and area of the droplet is also discussed based on the theory of liquid jet breakup, to build a dynamic breakup model of air resistance and broken jet. The jet trajectory of the fire water monitor is mainly influenced by the initial velocity, pitching angle, air resistance, and other factors. In this paper, the influence of different parameters on the jet drop point is considered. The analysis and comparison of all the points are performed, and the range of uncertainty is obtained. Finally, the accurate prediction of the jet trajectory is analyzed.

Keywords: Water jet; Universal grey number theory; Combinational algorithm; breakup; Fire water monitor.

NOMENCLATURE

A	cross-sectional area of the liquid jet, m^2
A_0	initial cross-sectional area of the liquid jet, m^2
C_D	coefficient of air resistance
C_{Di}	vortex drag coefficient
c_x	wave drag coefficient
F	air resistance force, N
f	wind drag, N
g	gravitational acceleration, m/s^2
H	maximum vertical height, m
h	the height of the nozzle, m
m	mass of the jet micro-body, kg

P	discharge pressure, MPa
Q	gas-water density ratio
q	discharge flow, kL/min
Re_{wg}	Reynolds number of liquid w and gas g
L	maximum horizontal range, m
T	Taylor number
U	relative velocity between the liquid drop and the gas, m/s
V	velocity of water jet, m/s
V_0	initial velocity of water jet, m/s
v_x	velocity component of the wind on the x-axis, m/s
We_{wg}	Weber number of water w and gas g
Z	Ohnesorge number
θ	discharge angle
β	angle of the water jet in motion in the horizontal direction
η	flow coefficient
ρ_{wg}	the density of water w and gas g, kg/m^3
μ	dynamic viscosity of water, m^2/s
σ	air-water surface tension, N/m.

1. INTRODUCTION

Fire water monitor is a crucial tool for firefighting. Modern fire is characterized by intense burning degree, fast spreading speed, high environmental temperature, and inaccessible fire personnel. Accordingly, the maximum efflux flow rate, horizontal range, and vertical shooting performance of the fire water monitor are proposed (Kolaitis *et al.*, 2014; Chen *et al.*, 2015). This paper mainly studies the shooting point of the fire water monitor, which mainly includes the prediction of the maximum horizontal range L and the maximum vertical height H (Whelan *et al.*, 2009). Li (2016) studied the effect of surface roughness on cavitations characteristics and energy loss under different inlet pressure and determined the optimum surface roughness through a large number of experiments. Min and Chen (2011) proposed a model of jet trajectory prediction considering the pitching angle of fire water monitor, which can effectively reduce the relative error between the measured value and the predicted value. Isaev (1966) developed an equation of the trajectory in a dragless case, which includes the Froude number Fr_d. Hatton and Osborne (1979) also agreed with this view and believed that if their model had a quadratic drag, then the Froude number would be a paramount parameter. But this is a problem obviously; if the air resistance coefficient is a fixed value, in the process of fluid movement, the air resistance is getting smaller and smaller because of the increasing speed, and it is obviously not in accordance with the actual situation. The hydrodynamic characteristics of a single and double coast lithotripsy breakwater under conventional and random waves are studied (Alkhalidi *et al.*, 2018). There are many factors affecting fire water monitor, such as air resistance, pitching angle, water jet speed, and other factors. Consequently, it is necessary to analyze the uncertainty. This work presents a new approach, known as universal grey system (or number) theory, for the first time to analyze jet water.

Grey numbers are proposed by Deng (1982) to deal with uncertainty and incomplete information. Then, they caught the attention of many scholars and scientific practitioners from around the world. The books by Liu and Lin (2006) summarized the various aspects of research and different types of applications in the area of grey systems. The focus of grey systems theory is uncertain problems with small samples and poor information that are difficult for probability to handle. The grey system theory deals with the study of grey numbers, grey parameters, and grey functions or grey relations (Liu *et al*., 2018). Grey systems theory was applied to several practical problems, such as information systems security (Shi *et al*., 2012), risk assessment of construction projects (Zavadskas *et al*., 2010), and multiple attribute decision making problems (Zhang *et al*., 2005). It can be seen that most of the applications of grey systems theory have been in non-engineering areas. In grey system theory, the partially known parameters are termed grey numbers. It can be seen that most of the applications of grey systems theory have been in non-engineering areas.

This article also introduces combinatorial algorithm approach to analyze uncertain variables. In this paper, the grey number theory and combinatorial algorithm are used to calculate and compare, combined with the results of studying and testing, the fire extinguishing effect, which is constantly improved.

This paper uses the grey number theory and combinatorial algorithm to simulate the trajectory of fire water monitor. These methods provide different boundaries of the output error and get deviations from the average. The paper consists of four major parts: Section 1 established the model of trajectory. Section 2 introduced the grey number theory and combinatorial algorithm. Section 3 is comparative analysis of numerical values. Section 4 concludes the paper.

2. JET TRAJECTORY EQUATIONS

The jet trajectory of the fire water monitor is mainly influenced by the initial velocity, discharge angle, air resistance, and other factors (in addition to the structure parameters of fire water monitor). In this study, the fire water jet is assumed to be an ideal fluid (no friction). The unit volume and unit flow of the fire water jet are investigated as research objects. The force analysis of the jet microbody is derived. As shown in Figure 1 and Figure 2, the tangential direction of the point on the jet trajectory is its velocity direction at that point. The resistance direction of the point is opposite to the velocity of the point. The tangential direction of each point on the jet trajectory is different (Figure 1). Consequently, the direction and magnitude of the air resistance and velocity are constantly changing.
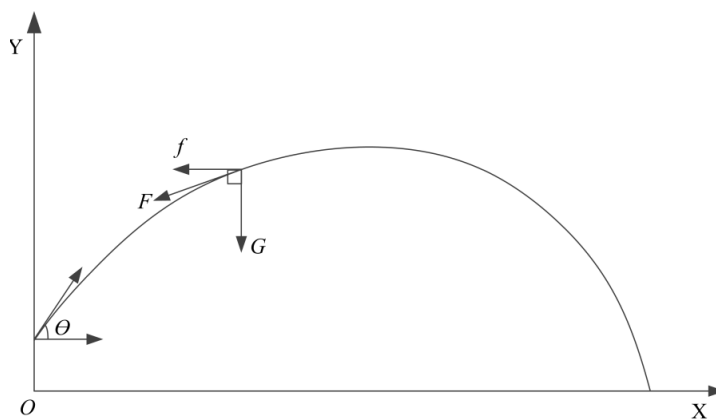
Figure 1. Schematic and coordinates of the jet.
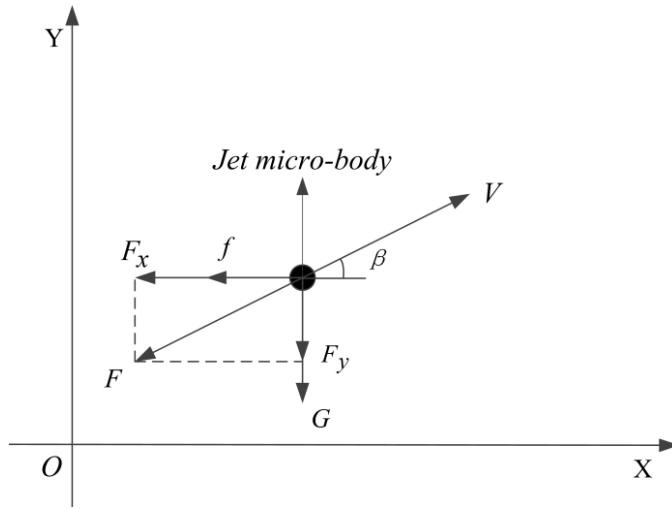
Figure 2. Vector diagram and representation of relative velocities.

The water jet is subjected to wind drag f, the component of air resistance force F in the X- and Y- directions, and gravity G (Figure 2). The initial conditions of the water jet include initial velocity V_0 and the angle θ between initial velocity and horizontal direction. Differential equations can be derived:

$$\frac{dx}{dt} = V_x = V \cos \beta, \tag{1}$$

$$\frac{dy}{dt} = V_y = V \sin \beta, \tag{2}$$

$$\frac{dV_x}{dt} = \frac{F_x}{m} \pm \frac{f}{m}, \tag{3}$$

$$\frac{dV_y}{dt} = \frac{F_y}{m} - g, \tag{4}$$

where V is the velocity of water jet, β is the angle of the jet in motion in the horizontal direction, m is the mass of the jet micro-body, g is the gravitational acceleration (9.81 m/s²), f is the wind drag, F is the air resistance, and subscripts x and y represent the force or velocity component in its direction.

On the basis of the above equations, the relationships among initial velocity V_0, discharge angle β, air resistance F, wind resistance f, and the jet trajectory of fire water monitor are necessary conditions for deriving the jet trajectory equation.

2.1. Drag model

In fluid dynamics, drag is the force that acts opposite to the relative motion of any moving object with respect to a surrounding fluid. This force can exist between two fluid layers (or surfaces) or a fluid and a solid surface. Drag force is proportional to the velocity for a laminar flow and to a squared velocity for a turbulent flow. Although the ultimate cause of a drag is viscous friction, turbulent drag is independent of viscosity drag forces, which always decrease the fluid velocity relative to the solid object in the fluid's path. Wind drag is the force that acts opposite to the relative motion of any moving object with respect to flowing air. The equations of wind pressure W_P and wind resistance f

under standard atmospheric pressure are $W_p = v^2/1600$ and $f = W_p \times A$, respectively. The direction of the wind is uncertain. The equation for wind resistance is

$$f = \frac{Av_x^2}{1600} \tag{5}$$

where v_x is the velocity component of the wind in the X-direction, and A is the cross-sectional area of the liquid jet.

The initial condition of the water jet is expressed as follows:

$$x\big|_{t=0} = 0, \ V_x\big|_{t=0} = V_0 \cos\theta$$
$$y\big|_{t=0} = 0, \ V_y\big|_{t=0} = V_0 \sin\theta \tag{6}$$

In general, the velocity of fire water monitor is considered to be faster than the low velocity missile. The quadratic drag model is used in this study. The air resistance force equation is

$$F = -\frac{\rho_g A C_D V^2}{2} \tag{7}$$

where C_D is the coefficient of air resistance, and ρ_g is the density of gas (1.2 kg/m³).

In this study, the air resistance of the fire water monitor mainly includes friction, vortex drag, and wave drag. No local shock wave is observed when the Mach number is less than 0.6. Therefore, the air resistance coefficient of the fire cannon jet is $C_D = \lambda + C_{Di}$ (Sun. 2009). Friction and vortex coefficients are

$$\lambda = \begin{cases} \dfrac{0.072}{\mathrm{Re}^{0.2}} & \mathrm{Re} \leq 10^6 \\ \dfrac{0.032}{\mathrm{Re}^{0.145}} & 10^6 \leq \mathrm{Re} \leq 10^{10} \end{cases}, \tag{8}$$

$$C_{Di} = \frac{0.029}{\sqrt{\lambda}}, \tag{9}$$

where $\mathrm{Re} = \rho U r/\mu$ is the Reynolds number, U is the relative velocity between the water drop and gas, and μ is the dynamic viscosity of water (1.002×10^{-6} m²/s).

On the basis of the force analysis in Figure 2, the equations for velocity component can be established as follows:

$$V_x = V\cos\beta - \frac{F}{m}t\cos\beta \pm \frac{f}{m}t$$
$$V_y = V\sin\beta - \frac{F}{m}t\sin\beta - gt \tag{10}$$

The displacement equations of the jet in the horizontal and vertical directions are

$$L = V \times t\cos\beta - \frac{F}{2m}t^2\cos\beta \pm \frac{f}{2m}t^2$$
$$H = V \times t\sin\beta - \frac{F}{2m}t^2\sin\beta \pm \frac{g}{2}t^2 \tag{11}$$

where L is the maximum horizontal range, and H is the maximum vertical height.

Water jet in air movement may break and constantly change the cross-sectional area. Moreover, the changes in the cross-sectional area of the jet can change air resistance. The force of air resistance and the magnitude and direction of jet velocity are closely related. Therefore, the angle between the velocities in the horizontal directions in Equation (10) and Equation (11), the water jet velocity, and the cross-sectional area of the jet constantly change, while the water jet moves in the air. In the case of the initial condition shown in Equation (6), air resistance and the cross-sectional area are assumed constant over a period of $\Delta t = 0.0001$ s. The horizontal and vertical displacements within 0.0001 s and the new velocity and air resistance of the water jet after 0.0001s can then be derived. The position of the microbody of the flow is determined by the accumulation of the displacement in the horizontal and vertical directions. The jet trajectory curve of the fire water monitor can then be obtained.

2.2. Cross-sectional area model

Liquid jet breakup has two forms, namely, breakup and atomization. These forms might exist simultaneously in the breakup process of liquid jet. Rayleigh (1878) conducted an experimental study on liquid jet and found that the disturbance of gas would lead to liquid jet breakup. Weber (1931) proposed an unstable model formed by the aerodynamic interaction of low-velocity viscous and nonviscous circular jet on the gas–liquid interface and proposed an important, dimensionless parameter, namely, the Weber number, in atomization theory. O'Rourke and Bracco (1980) divided the spray field into different areas, as shown in Figure 3. Lebas et al. (2009) investigated the atomization process of high-velocity water jet and analyzed the initial atomization process of two liquid jet models through numerical simulation.
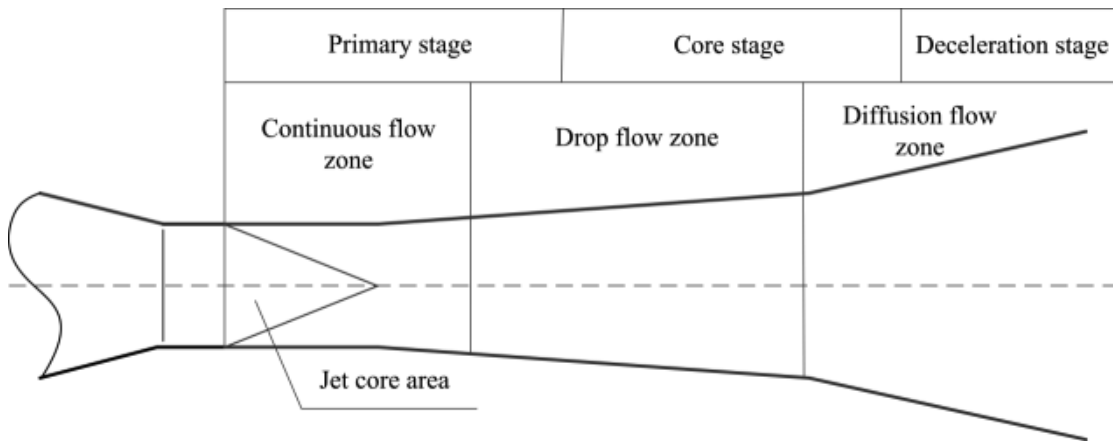
Figure 3. Breakup process of fire water jet monitor.

After the water jet enters the air, the stability of the gas–liquid surface will begin to break because of the internal surface tension, viscous force, gravity, and air resistance of the water jet (Suñol *et al.*, 2015). The development stage of liquid jet breakup is caused by the gradual increase of the self-viscosity force of liquid drops in the process of breaking-up, the diameter and velocity of droplets are reduced, and the gas–liquid surface will gradually become stable; therefore, the droplets are no longer broken. A new dimensionless parameter *Je* was proposed to distinguish the breakup and atomization modes. This model considers $Je = 1$ as the critical condition between crushing and atomization. When the jet is atomized, the radius of the droplet is smaller; thus, the atomization is assumed to have no effect on the cross-sectional area of the jet. The dimensionless parameter can be calculated as follows:

$$Je = \frac{We}{Q} = \frac{2\sigma}{\rho_g U^2 d},$$
(12)

where $We = \rho_w U^2 r / \sigma$ is the Weber number, σ is the surface tension of water (7.2×10^{-2} N/m), and Q is the gas–liquid density ratio.

Reitz (1987) considered the Rayleigh–Taylor and Kelvin–Helmholtz (K–H) instability waves as breakup factors of the droplet. The WAVE model presumed that new droplets with radius r_c and r_b were broken from a parent parcel with radius r, such that

$$r_c = B_0 \Lambda_{wave} \ , \ r_b = \left(r^3 - r_c^3\right)^{1/3}, \tag{13}$$

where Λ_{wave} is the wavelength, and B_0 is a constant equal to 0.61. The frequency of the fastest growing wave and its corresponding wavelength can be calculated as follows:

$$\Omega_{wave} = \frac{0.34 + 0.385 We_g^{1.5}}{(1+Z)(1+1.4T^{0.6})} \sqrt{\frac{\sigma}{\rho_w r^3}}, \tag{14}$$

$$\Lambda_{wave} = \frac{9.02r\left(1 + 0.45\sqrt{Z}\right)\left(1 + 0.4T^{0.7}\right)}{\left(1 + 0.865 We_g^{1.67}\right)^{0.6}}, \tag{15}$$

where Z is the Ohnesorge number, $Z = \sqrt{We_w}/\mathrm{Re}_w$; ρ_w is the density of water (1000 kg/m³); Re_w is the Reynolds number of water, $\mathrm{Re}_w = \rho_w U r / \mu$; and T is the Taylor number, $T = Z\sqrt{We_g}$.

The experiments of Patterson and Reitz (1998) showed that a parent parcel might decompose a new droplet with a radius larger than that of the parent parcel.

$$r_c = \begin{cases} B_0 \Lambda_{wave} & B_0 \Lambda_{wave} \le r \\ \min \begin{bmatrix} 3\pi r^2 U / 2\Omega_{wave} \\ \left(3r^2 \Lambda_{wave}/4\right)^{0.33} \end{bmatrix} & r < B_0 \Lambda_{wave} \end{cases} \tag{16}$$

The equation for the breakup time of bag at low Weber numbers and the stripping breakup at high Weber numbers can be calculated as follows (Reitz *et al.*, 1987):

$$\tau_{wave} = \frac{3.72 B_1 r}{\Omega_{wave} \Lambda_{wave}} \tag{17}$$

where B_1 is a constant that causes differences in the drop breakup time due to the differences in the initial conditions. The value of B_1 will be affected by the upstream conditions of the nozzle, such as L/D ratio and cavitation at high injection pressures. However, in the present study, B_1 is set to 1.73, as recommended by Orourke and Amsden (1987).

This study assumes that no air gap exists between the new droplets after the water jet is broken. Therefore, the cross-sectional area of the two new droplets is

$$A = \pi\left(r_b^2 + r_c^2\right) \tag{18}$$

The change rate of the cross-sectional area within 0.0001 s can be derived from Equation (17) and Equation (18).

$$\Delta A = \frac{r_b^2 + r_c^2}{r^2} \tag{19}$$

This study assumes that the droplets are continuously broken; thus, a new cross-sectional area and air resistance can be obtained after every 0.0001 s. $Je = 1$ and $H = 0$ are used as boundary conditions for programming. The program flowchart is shown in Figure 4.
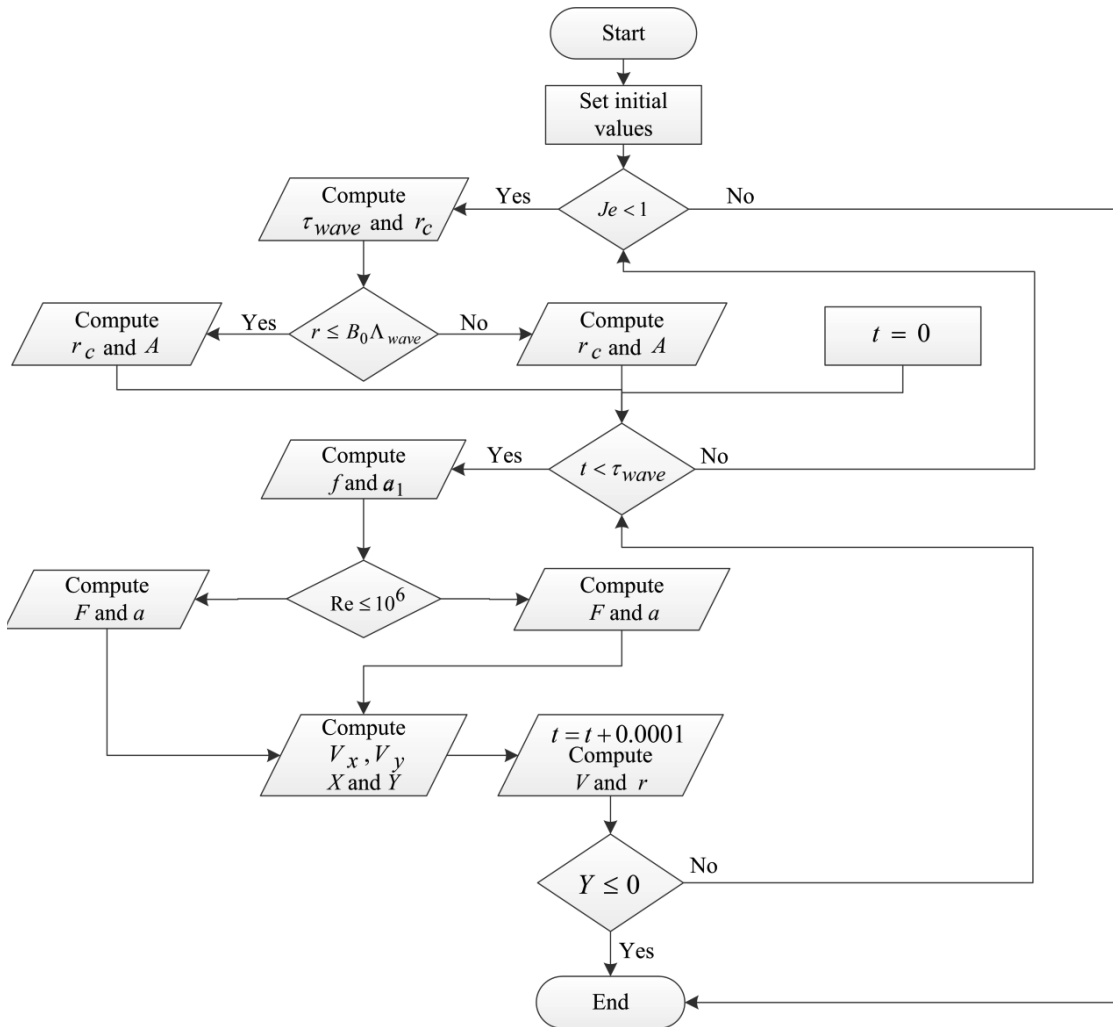
Figure 4. Program flowchart of the dynamic breakup model of air resistance and broken jet.

3. GREY SYSTEM FOR JET

Grey system A grey number is a number whose value is unknown among a set of continuous numbers that have clearly defined lower and upper bounds. A grey number x can be expressed as $x = \left[\underline{x}, \overline{x}\right] = \left\{t / \underline{x} \le t \le \overline{x}\right\}$, where t denotes the information with $\underline{x}$ and $\overline{x}$ as the lower and upper bounds of the information, respectively. Thus, a grey number is represented in terms of its possible range of variation.

3.1. Universal grey number theory

A general function f can be denoted as a universal grey number with lower and upper bounds as follows:

$$f = \left[\underline{f}, \overline{f}\right] = (\overline{f}, \left[\frac{\underline{f}}{\overline{f}}, 1\right])$$ (20)

In this paper, the point range of uncertain parameters is analyzed by using universal grey theory. The comparison of the number of grey and the combination method uses the same interval values. This work presents a new method, the grey system (or number) theory, which is the first time to analyze an uncertain jet water parameter.

Equation (5) can be rewritten as universal grey system relations as follows:

$$\left(\overline{f}, \left[\frac{f}{\overline{\overline{f}}}, 1\right]\right) = \frac{A\left(\overline{v_x^2}, \left[\frac{v_x^2}{\overline{\overline{v_x^2}}}, 1\right]\right)}{1600} \tag{21}$$

Equation (7) can be expressed as follows:

$$\left[\underline{F}, \overline{F}\right] = -\frac{\rho_g\left[\underline{A}, \overline{A}\right] C_D \left[\underline{V}, \overline{V}\right]^2}{2} \tag{22}$$

Equation (10) can be rewritten as follows:

$$\left(\overline{V_x}, \left[\frac{V_x}{\overline{\overline{V_x}}}, 1\right]\right) = \left(\overline{V}, \left[\frac{V}{\overline{\overline{V}}}, 1\right]\right)\cos\beta - \frac{F}{m}t\cos\beta \pm \frac{f}{m}t$$

$$\left(\overline{V_y}, \left[\frac{V_y}{\overline{\overline{V_y}}}, 1\right]\right) = \left(\overline{V}, \left[\frac{V}{\overline{\overline{V}}}, 1\right]\right)\sin\beta - \frac{F}{m}t\sin\beta - gt \tag{23}$$

Equation (11) can be expressed as follows:

$$\left(\overline{L}, \left[\frac{L}{\overline{\overline{L}}}, 1\right]\right) = \left(\overline{V}, \left[\frac{V}{\overline{\overline{V}}}, 1\right]\right) \times t\cos\left(\overline{\beta}, \left[\frac{\beta}{\overline{\overline{\beta}}}, 1\right]\right) - \frac{F}{2m}t^2\left(\overline{\beta}, \left[\frac{\beta}{\overline{\overline{\beta}}}, 1\right]\right) \pm \frac{\left(\overline{f}, \left[\frac{f}{\overline{\overline{f}}}, 1\right]\right)}{2m}t^2$$

$$\left(\overline{H}, \left[\frac{H}{\overline{\overline{H}}}, 1\right]\right) = \left(\overline{V}, \left[\frac{V}{\overline{\overline{V}}}, 1\right]\right) \times t\sin\left(\overline{\beta}, \left[\frac{\beta}{\overline{\overline{\beta}}}, 1\right]\right) - \frac{F}{2m}t^2\left(\overline{\beta}, \left[\frac{\beta}{\overline{\overline{\beta}}}, 1\right]\right) \pm \frac{g}{2m}t^2 \tag{24}$$

3.2. Solution using combinatorial approach

In general, the combinatorial approach can be used to find the range of any arbitrary function f of several imprecise parameters or variables by considering all possible combinations of lower and upper bounds of all the variables and evaluating the value of f at each combination of the parameters or variables. For this, let the function be given by $f(x_1, x_2 \cdots x_n)$ with each variable x_i denoting an interval number. By considering the lower and upper bounds of x_i as follows:

$$x_i = [\underline{x_i}, \overline{x_i}] = [x_1^{(i)}, x_2^{(i)}] \tag{25}$$

The various possible combinations of lower and bounds of all n variables can be used to evaluate f as follows:

$$f_r = f\left(x_1^{(i)}, x_2^{(j)} \dots x_n^{(k)}\right); i = 1, 2; j = 1, 2; r = 1, 2, 3 \dots 2^n \tag{26}$$

where f_r notes the value of f for a specific combination of the lower and upper bounds of the intervals of $x_1, x_2 \dots x_n$. The combinatorial algorithm is not introduced in detail.

4. SIMULATION ANALYSIS

The experimental parameters and data in Sun (2009) were used for simulation. The experimental conditions in Sun (2009) are as follows: temperature of $15°C \sim 20°C$, wind speed is third to fourth levels: the fire water monitor from the ground is 5 meters high, the three-level wind is 3.4~5.5 m/s, and level 4 wind is 5.5~8.0 m/s. From what has been discussed above, we select the wind speed 5 m/s, and bias is 5% m/s, pitching angles from 30°, 45°, 60° simulation algorithm for universal grey number and combinatorial approach in the angular deviation of ±2°, then we choose

different initial velocities to carry out three cases: deterministic analysis (DA), universal grey system theory (UGST), and combinational analysis (CA).

Table 1. Experimental parameters of water jet.

Experimental parameters	Experience 1	Experience 2	Experience 3
q (L/s)	50.4	67.5	79.4
A_0 (m²)	0.00098058	0.00121270	0.00147334
r (m)	0.01766715	0.01964725	0.02165592
V_0 (m/s)	51.3965	55.7001	53.8724
P (MPa)	1.27	1.46	1.4

Case 1

The velocity of fire water jet was 51.3965 m/s, and the universal grey number and combinatorial algorithm both choose bias 5 m/s. The case 1 parameters are shown in Table 1.

In Table 1, the jet trajectories are simulated at different pitching angles, air resistance, and initial as shown in Figure 5, Figure 6, and Figure 7.
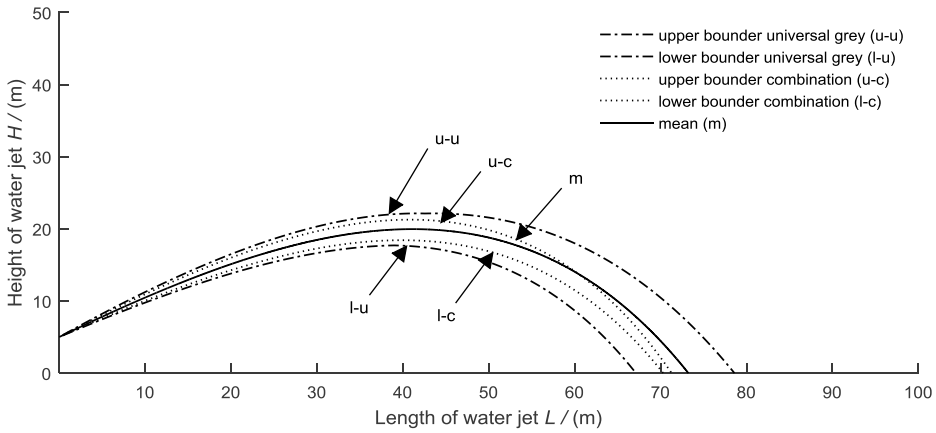
Figure 5. Trajectory of water jet in different approaches ($\theta = 30°$).
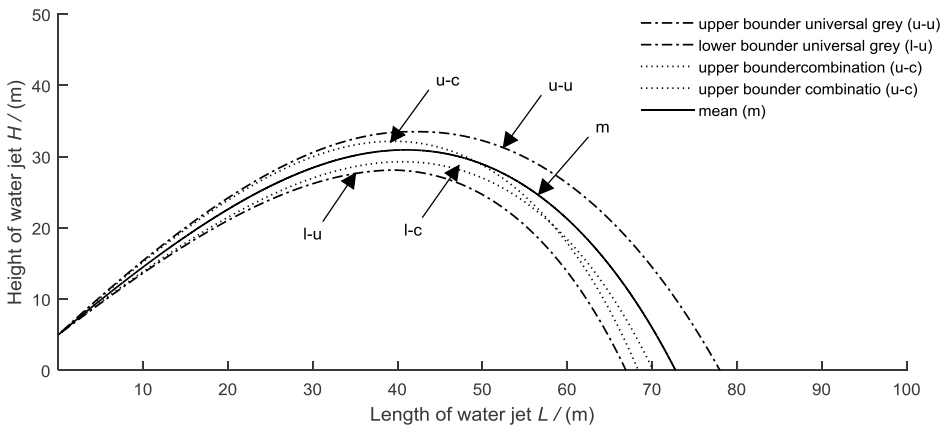
Figure 6. Trajectory of water jet in different approaches ($\theta = 45°$).
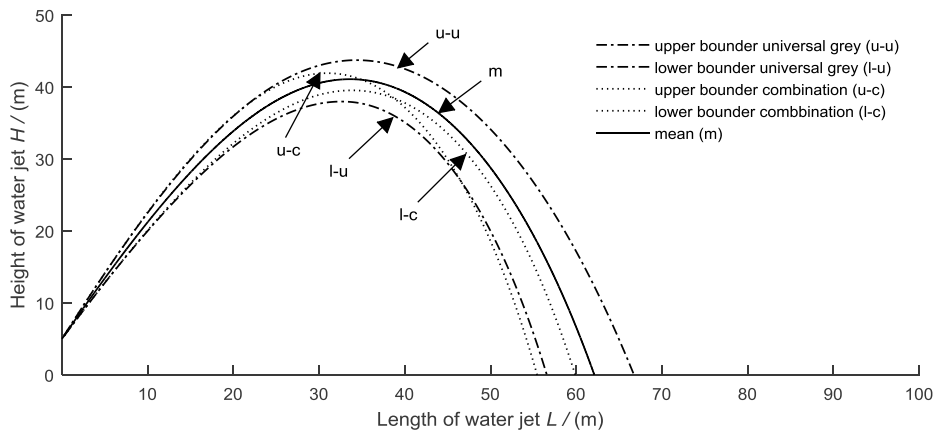
Figure 7. Trajectory of water jet in different approaches ($\theta = 60°$).

Figure 5 shows a pitching angle of 30°, wind speed of 5±5% m/s, and jet velocity of 51.3965 m/s. It can be seen from the figure that the universal grey theory has a large range of points, and width is about 11.5459 m, while the range of the combinatorial algorithm is small, as far as 73.2334 m, the nearest is about 70.3368 m, and error width is 0.9755 m approximately. The upper boundary of the universal grey number is 22.1409 m, and the highest point of lower boundary is 17.7019 m, while the upper boundary of the combinatorial algorithm is 21.2706 m, and the highest point of the lower boundary is 18.4215 m. Determine the value of the highest point to be 19.959 m, and at (60.4917, 13.7066) determine the value of parabolic intersection with upper bound combinatorial algorithm, because a combinatorial cap of 2° angle is higher than certain value and, thus, will drop in advance. There is a detailed comparison between simulated data and experimental data in Table 2.

Figure 6 shows a pitching angle 45°, initial velocity 51.3965±5% m/s, and wind speed 5±2 m/s. As can be seen from the figure, the upper and lower boundaries of the universal grey number are falling steadily, while the combinatorial algorithm intersects the lower boundary at (58.2296, 20.4748). In (49.2967, 29.2541), the upper boundary of the combinatorial algorithm intersects with the determined value and combinatorial algorithm, where the width is 1.8161 m, universal grey number width is 11.1578 m, combination algorithm is the upper limit of the highest point 32.1622 m, and the highest point of the lower boundary is 29.2907 m. The upper boundary of the universal grey is 33.5028 m, the lower boundary is 39.4709 m, and the highest point of the mean is 30.9524 m.

Figure 7 shows three methods of jet trajectory diagram, where the pitching angle is 60°±2°, jet velocity is 51.3965±5% m/s, and wind speed is 5±2 m/s. It can be seen from the figure that the universal grey shows two stable parabola points. The combinatorial algorithm has two parabolas intersecting at (38.7181, 38.4469), and at (34.9959, 41.0011) the legal upper limit and the determined value intersect, and the upper boundary of the combinatorial algorithm at (46.5325, 26.9449) intersects the lower bound of the universal grey number .The highest point of the upper boundary of grey limit is 43.7264 m, the highest point of the lower limit is 37.9737 m, the upper boundary of the combinatorial algorithm is 41.9166 m, and the upper limit is 39.5311 m. In the combinatorial algorithm, the point width is 4.4522 m, and the width of the grey algorithm is 10.1799 m.

Table 2 shows the fire water monitor in jet speed 51.3965±5%m/s, wind speed 5±5% m/s, at angles 30°, 45°, 60° under the condition of maximum level range and the maximum vertical range, respectively. Some differences are observed between the simulated and experimental jet trajectories because of the interference of the wind and the error of the pitching angle when the experimental data are measured. The simulation data of this model and the simulation data in Sun (2009) show a large error in the maximum vertical height of the discharge angle at 60° in experience. This error might be caused by the existence of a great deviation when the experimental data were measured or recorded. We can see that the experimental conditions of pitching deviation angle 2° directly affect the jet trajectory.

In contrast, the model and simulation show that the model fitting degree of the universal grey number is better, the error is more stable, and it is closer to the mean of the experimental value.

Table 2. Comparison of the simulation and experimental data of water jet.

θ(°)	Approach		L(m)	Error[a]	H(m)	Error[a]
		Exp	66	-	16.85	-
30	DA	Sim[b]	72.3	9.55%	16.7	0.89%
		Sim[c]	73.2334	10.96%	19.9594	18.45%
	UGST	Sim[c]	[67.1299, 78.6758]	[1.71%, 19.21%]	[17.7019, 22.1409]	[5.05%, 31.4%]
	CA	Sim[c]	[70.3368, 71.3123]	[6.57%, 8.05%]	[18.4215, 21.2706]	[9.33%, 26.24%]
		Exp	61	-	26.6	-
45	DA	Sim[b]	71.2	16.67%	29.4	10.53%
		Sim[c]	72.7609	19.28%	30.95241349	23.88%
	UGST	Sim[c]	[66.9172, 78.0750]	[9.70%, 27.99%]	[39.4709, 33.5029]	[48.37%, 25.95%]
	CA	Sim[c]	[68.3770, 70.1931]	[12.09%, 15.07%]	[29.2907, 32.1622]	[10.12%, 20.91%]
		Exp	56	-	29.7	-
60	DA	Sim[b]	60.7	7.74%	42.5	43.09%
		Sim[c]	62.1103	10.91%	41.0837	38.33%
	UGST	Sim[c]	[56.5689, 66.7488]	[1.02%, 19.19%]	[37.9737, 43.7264]	[27.86%, 32.08%]
	CA	Sim[c]	[55.4483, 59.9005]	[9.6%, 6.97%]	[39.5311, 41.9166]	[33.10%, 41.13%]

Error[a]: the error between simulation data and experimental data;

Sim[b]: the simulation data from Sun (2009);

Sim[c]: the simulation data in this paper.

Case 2

The experimental parameters and experimental data in the Sun (2009) are used for simulation verification. The same as the experimental conditions of case 1, the velocity of the water jet is 55.7001 m/s, and the pitching angle is from 30°, 45°, 60°, respectively. The experimental parameters are shown in Table 1.

According to the experimental parameters of Table 1, water jet angles of 30°, 45°, 60°, and universal grey and combinatorial algorithm for simulation of the available water jet trajectory are shown in Figure (8), (9), and (10).
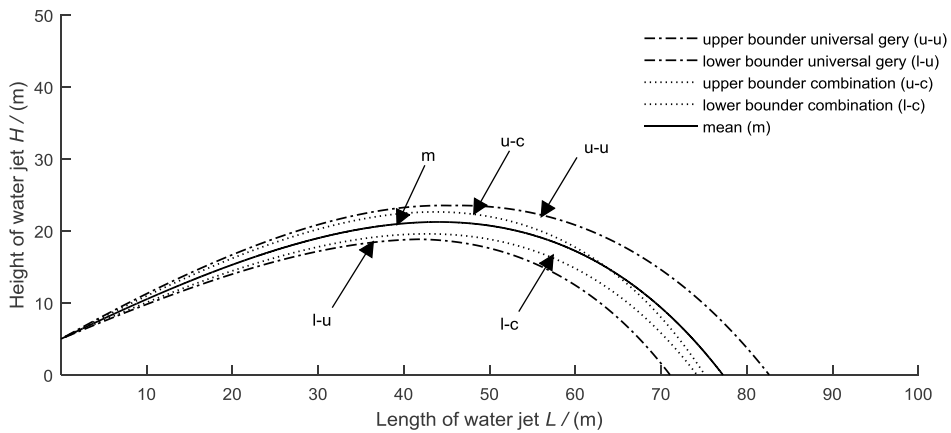
Figure 8. Trajectory of water jet in different approaches ($\theta = 30°$).
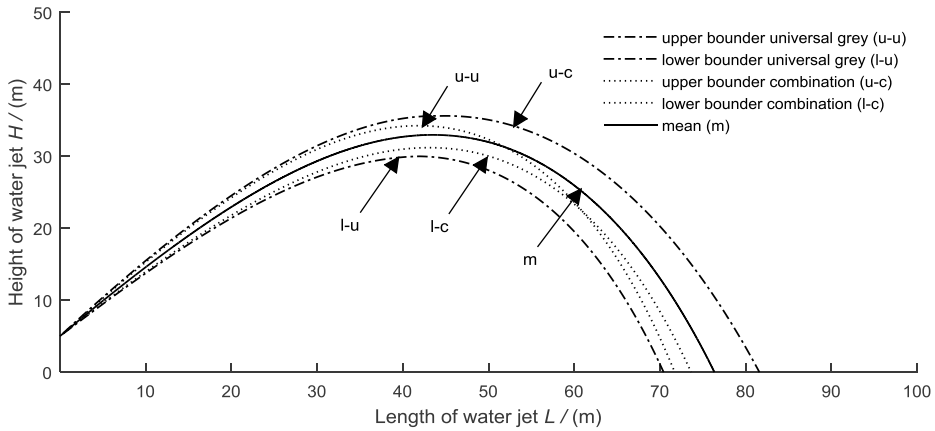
Figure 9. Trajectory of water jet in different approaches ($\theta = 45°$).
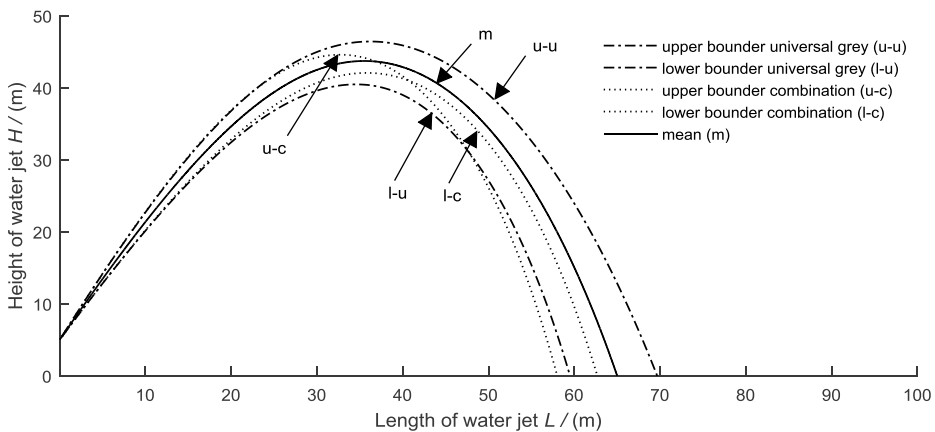
Figure 10. Trajectory of water jet in different approaches ($\theta = 60°$).

From the perspective of Figure 8 in 30°±2°, jet velocity is 55.7001±5% m/s, a wind speed of 5±2 m/s can be seen from the diagram, and there is a placement of a universal grey width of 11.5617 m. The combinatorial algorithm has a point width of 0.9194 m. The upper bounder of the universal grey algorithm is 23.5361 meters, the lower

limit is 18.8427 meters, the upper limit of the combinatorial algorithm is 22.6407 meters, and the lower limit of the combinatorial algorithm is 19.5913 m. At (63.6693, 14.8971), the upper bound of the combinatorial algorithm intersects the deterministic value.

Figure 9 shows the conditions of the jet trajectories, with a jet velocity 55.7001±5% m/s, angle 45°±2°, air resistance 5±2 m/s, and the change trend of parabola obtained by three methods is shown. But from the table, the range of error is further expanded. The upper bound parabola obtained by universal grey is generally higher than that of the combinatorial algorithm and the determination value algorithm, and the grey algorithm shows two stable parabolas. At the point (60.9272, 22.3661), the combinations of the upper limit and the lower limit intersect. At (51.9130.31.2616), the mean value is intersected with the upper limit of the combinatorial algorithm. The width of the grey algorithm is 11.2253 m, and the width of the combinatorial algorithm is 1.9558 m.

From the perspective of Figure 10 of 60°±2°, jet speed is 55.7001±5% m/s, the wind speed can be seen in the 5±2 m/s, universal grey on parabolic values was greater than combinatorial algorithm, grey algorithm was running smoothly, as well as the combinatorial algorithm after running a certain distance, due to gravity at (36.8673, 36.8673), the combinatorial algorithm is of maximum and average intersection, at (40.6846, 40.6846), the combinatorial algorithm is the upper limit and lower limit of intersection, and at (47.7076, 47.7076), the upper limit and the lower limit of grey-scale algorithm of the combinatorial algorithm were shown.

Table 3. Comparison of the simulation and experimental data of water jet.

$\theta(°)$	Approach		L (m)	Error[a]	H (m)	Error[a]
		Exp	77	-	20.2	-
30	DA	Sim[b]	81.7	6.10%	18.8	6.93%
		Sim[c]	77.2080	0.27%	21.2449	5.17%
	UGST	Sim[c]	[71.0439, 82.6056]	[7.74%, 7.28%]	[18.8427, 23.5361]	[6.72%, 16.52%]
	CA	Sim[c]	[74.2182, 75.1376]	[3.61%, 2.42%]	[19.5913, 22.6407]	[3.01%, 12.08%]
		Exp	72	-	29.3	-
45	DA	Sim[b]	80.8	12.22%	32.7	11.60%
		Sim[c]	76.3521	6.04%	32.9669	12.52%
	UGST	Sim[c]	[70.4251, 81.6504]	[2.19%, 13.40%]	[29.9891, 35.6048]	[2.35%, 21.52%]
	CA	Sim[c]	[71.7411, 73.6969]	[0.36%, 2.36%]	[31.1906, 34.2426]	[6.5%, 16.87%]
		Exp	67	-	37.1	-
60	DA	Sim[b]	68.2	1.79%	47.9	29.11%
		Sim[c]	64.9976	2.99%	43.7135	17.83%
	UGST	Sim[c]	[59.4985, 69.7002]	[11.20%, 4.03%]	[40.4657, 46.4178]	[9.07%, 25.12%]
	CA	Sim[c]	[58.0404, 62.6924]	[13.37%, 6.43%]	[42.0587, 44.5836]	[13.37%, 20.17%]

Error[a]: the error between simulation data and experimental data;

Sim[b]: the simulation data from Sun (2009);

Sim[c]: the simulation data in this paper.

Table 3 shows the fire water cannon in jet speed 55.7001 m/s, a wind speed of 5 m/s, under angles 30°, 45°, 60°, and the condition of maximum level range and the maximum vertical range, respectively.

Case 3

The experimental parameters and experimental data are used for simulation verification (O'Rourke et al., 1980). In the same experimental condition as case 1 and case 2, the wind speed selected 5 m/s deviation to ±5 m/s, and the water jet velocity was 53.8724 m/s, and the experimental parameters at pitching angles 30°, 45°, 60°, respectively, are shown in Table 1.
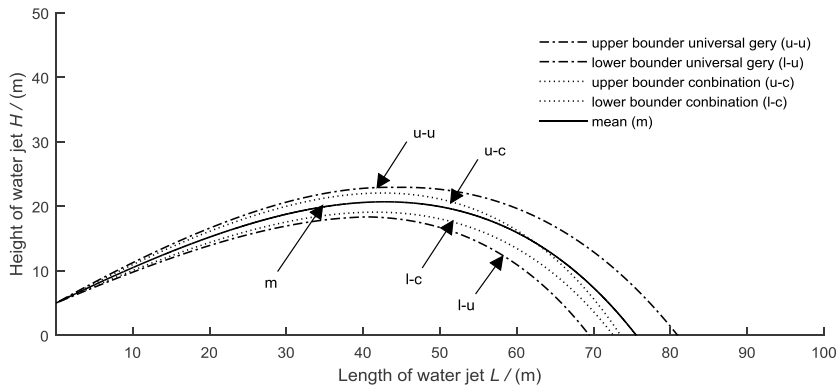
Figure 11. Trajectory of water jet in different approaches ($\theta = 30°$).
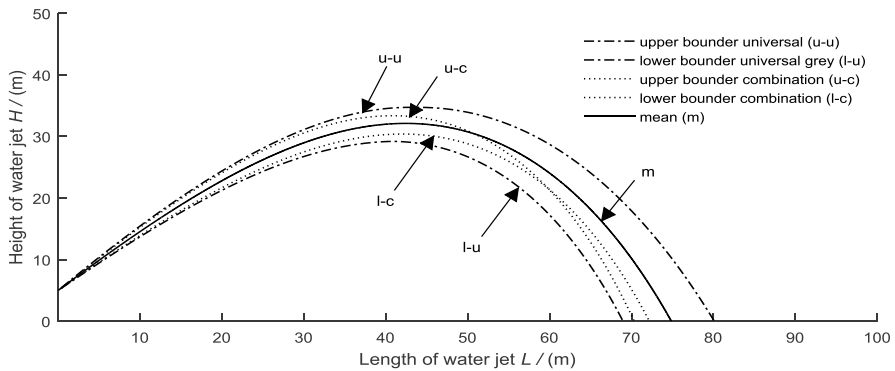
Figure 12. Trajectory of water jet in different approaches ($\theta = 45°$).
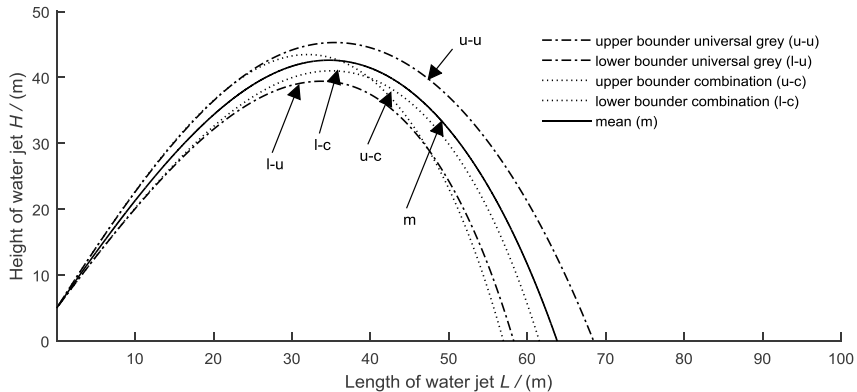
Figure 13. Trajectory of water jet in different approaches ($\theta = 60°$).

Figure 11 shows an angle 30°±2°, jet speed 53.8724±5% m/s, and wind speed 5±2 m/s. It can be seen from the figure that the upper combination value of the universal grey is the highest, the lower boundary is the lowest, the width of the falling point is about 20.229 m, and the upper boundary of the combinatorial algorithm at (62.3585,14.3910) intersects with the deterministic. The combinatorial algorithm of ceiling on point 73.5880 m, combinatorial algorithm where the width is 0.9843 m, and grey algorithm where the width is 20.229 m, combinatorial algorithm of maximum peak of 22.0669 m, lower peak of 19.1009 m, and the maximum grey algorithm for high 22.9522 m, the minimum peak of 18.3627 m, and mean peak 20.7060 m are shown.

Figure 12 shows that 45°±2° angle, jet speed 53.8724±5% m/s, and wind speed 5 ±5 m/s can be seen from the diagram, as well as a grey line on top of the algorithm and the lowest limit, two parabolic stabilities of the grey level steadily falling in (50.8097, 50.8097) after the intersection in combination of upper and lower limits. Ceiling is on 70.3882 meters, the lower limit is on 72.1869 meters, at (50.8294, 50.8294), after the maximum combinatorial algorithm of fellowship with average, average fell on the point is 74.8652 meters, grey algorithm of line on the highest point is 34.7296 meters, the boundaries of the highest point are 29.2082 meters, the combinatorial algorithm of line is 33.3735 meters, the highest point of limits is 30.3966 meters, the width of the grey-scale algorithm is larger, about 11.2244 meters, and the combinatorial algorithm of placement of a smaller width is 1.7987 meters.

As can be seen from Figure 13, the angle is 60°±2°, jet velocity is 53.8724 ±5% m/s, the wind speed is 5±2 m/s, universal grey theory was higher than the upper boundary value of combinatorial algorithm, at (39.8744,39.8744), the combinatorial algorithm after the upper bound and lower bound of the intersection is shown, ceiling is on point (56.9962, 0), the lower limit is on (61.5410, 0), at (36.0960, 36.0960), the upper boundary of the combinatorial algorithm with the average intersection is shown, the average falls in point (63.8055, 0), placement of universal grey theory width is 10.2126 meters, and the combinatorial algorithm where the width is 4.5448 meters is shown.

Table 4. Comparison of the simulation and experimental data of water jet.

θ(°)	Approach		L(m)	Error[a]	H(m)	Error[a]
30		Exp	82	-	21	-
	DA	Sim[b]	84.7	3.29%	19	9.52%
		Sim[c]	75.5588	7.86%	20.70601504	1.40%
	UGST	Sim[c]	[60.7409, 80.9699]	[25.92%, 1.26%]	[18.3627, 22.9522]	[12.56%, 9.30%]
	CA	Sim[c]	[72.6037, 73.5880]	[11.46%, 10.26%]	[19.1009, 22.0669]	[9.04%, 5.08%]
45		Exp	76	-	36	-
	DA	Sim[b]	84.1	10.65%	33.7	6.39%
		Sim[c]	74.8652	1.94%	32.12487960	10.76%
	UGST	Sim[c]	[68.9676, 80.1920]	[9.25%, 5.52%]	[29.2082, 34.7296]	[18.87%, 3.53%]
	CA	Sim[c]	[70.3882, 72.1869]	[7.38%, 5.01%]	[30.3966, 33.3735]	[15.57%, 7.30%]
60		Exp	70	-	50.2	-
	DA	Sim[b]	71.2	1.71%	48.7	2.99%
		Sim[c]	63.8055	8.85%	42.6161	15.11%
	UGST	Sim[c]	[58.2681, 68.4807]	[16.76%, 2.17%]	[39.4255, 45.2954]	[21.46%, 9.77%]
	CA	Sim[c]	[56.9962, 61.5410]	[18.58%, 12.08%]	[41.0045, 43.4716]	[18.32%, 13.40%]

Error[a]: the error between simulation data and experimental data;

Sim[b]: the simulation data from Sun (2009);

Sim[c]: the simulation data in this paper.

5. CONCLUSIONS

In this paper, the jet trajectory of the fire water monitor is taken as the research object, and the jet trajectory differential equation is established according to particle kinematics and crushing theory. Considering the influence of parameter uncertainty in the jet process, the target uncertainty is studied. The main conclusions are as follows:

(1) By analyzing the jet path of the fire water cannon, the jet water column of the fire water cannon is compared with the continuous motion of a single particle to establish the jet path differential equation. The air resistance coefficient and jet cross-sectional area are determined according to the law of droplet movement in the air. A dimensionless parameter Je is used to determine the breaking and atomizing state of droplets, and the range and height models are established. The simulation results of the jet trajectory model are compared with the experimental results to verify the accuracy of the model.

(2) Considering the parameter uncertainties in the actual jet, such as the initial velocity V_0, discharge angle θ and wind speed v of the jet, the uncertain parameters are simulated by using the grey algorithm and the combined algorithm to obtain the uncertain jet trajectory curve. In three case experiments, the results of the two uncertainty algorithms show that the expansion degree of the combined algorithm is lower than that of the grey algorithm.

(3) Although the combination method gives a small degree of expansion, most practical structures involve hundreds of uncertain parameters. Therefore, it becomes almost impractical to use the combinatorial approach. The proposed universal grey number theory has been shown to be free of the dependency problem. Analyzing the reasons for the expansion of different algorithms can predict the uncertain trajectory of the fire water monitor in the actual project effectively, and the method is also applicable to other uncertain projects.

ACKNOWLEDGMENT

REFERENCES

Alkhalidi, M.A., Neelamani, S . & Al-Zagah, Z. 2018. Hydrodynamic characteristics of single and twin offshore rubble mound breakwaters under regular and random waves. Journal of engineering research, **6**(1): 1-16.

Chen, H., Pittman, W.C. & Hatanaka, L.C. 2015. Integration of process safety engineering and fire protection engineering for better safety performance. Journal of Loss Prevention in the Process Industries, **37**:74-81.

Deng, J.L. 1982. The Control Problem of Grey Systems. Systems & Control Letters, **1**(5): 288-294.

Hatton, A.P. & Osborne, M.J. 1979. The Trajectories of Large Fire Fighting Jets. International Journal of Heat and Fluid Flow, **1**(1): 37-41.

Isave, A.P. 1966. Optimal'nyye rezhimy raboty dal'nos-truynykh dozhdeval'nykh mashin (Optimal operating conditions of long-range sprinklers). Mekhanizatsiyai elektrifikatsiya sots-ialisticheskogo sel'skogo khozyaystva. **24**(9): 4-9.

Kolaitis, D.I., Asimakopoulou, E.K. & Founti, M.A. 2014. Fire protection of light and massive timber elements using gypsum plasterboards and wood based panels: A large-scale compartment fire test. Construction & Building Materials, **73**: 163-170.

Lebas, R., Menard, T., Beau, P.A., Berlemont, A. & Demoulin, F.X. 2009. Numerical simulation of primary break-up and atomization: DNS and modeling study. Int. J. Multiphase Flow, **35**(3): 247-260.

Li, D., Kang, Y. & Wang, X. 2016. Effects of nozzle inner surface roughness on the cavitation erosion characteristics of high speed submerged jets. Experimental Thermal & Fluid Science, **74**: 687-757.

Liu, S.F & Lin, Y. 2006. Grey Information: Theory and Practical Applications. kybernetes, 2006, **37**(1):189-189.

Liu, X.T. & Rao, S.S. 2018. Vibration Analysis in the Presence of Uncertainties Using Universal Grey System Theory. Journal of Vibration & Acoustics, **140**(3):031009.1-031009.11.

Min, Y.L. & Chen, X.Y. 2011. Pitching angle-based theoretical model for the track simulation of water jet out from water fire

monitors. Journal of Mechanical Engineering. **47**(11): 134-138.

Orourke, P.J. & Amsden, A.A. 1987. The TAB method for numerical calculation of spray droplet breakup. SAE Paper. No.872089

O'Rourke, P.J. & Bracco, F.V. 1980. Modeling of drop interactions in thick sprays and a comparison with experiments. Proc. Inst. Mech. Eng, **9**: 101-116.

Patterson, M.A., & Reitz, R.D. 1998. Modeling the effects of fuel spray characteristics on diesel engine combustion and emissions, SAE Transactions. **106**(3): 27-43.

Rayleigh, L. 1878. On the instability of jets, Proc. London Math. Soc. **10**: 4-13.

Reitz, R.D. 1987. Modeling atomization processes in high-pressure vaporizing sprays. Atomization & Spray Tech. **3**(309): 309-337.

Reitz, R.D. & Diwakar, R. 1987. Structure of high-pressure fuel sprays. SAE Transactions, **96:** 492-509.

Shi, H. & Deng, Y. 2012. A Grey Model for evaluation of Information Systems Security. Journal of Computer, **7**(1): 284-291.

Sun, J. 2009. Research of the Trajectory of Fire-fighting Monitor's Jet, Shanghai: Shanghai Jiao Tong University.

Suñol, F. & Gonzálezcinca, R. 2015. Liquid jet breakup and subsequent droplet dynamics under normal gravity and in microgravity conditions, Physics of Fluids, **27**(7): 077102 .

Weber, C. 1931. Disintegration of liquid jets, Z. Angew. Math. Mech. **11**(2): 136-159.

Whelan, B.P. & Robinson, A.J. 2009. Nozzle geometry effects in liquid jet array impingement. Applied Thermal Engineering, **29**(11/12): 2211-2221.

Zavadskas, E.K., Turskis, Z. & Tamosaitience, J. 2010. Risk Assessment of Construction Projects. Journal of Civil Engineering and Management, **16**(1): 33-46.

Zhang, J.J., Wu, D.S. & Olson, D.L. 2005. The Method of Grey Related Analysis to Multiple Attribute Decision Making Problems through Interval Numbers. Mathematical and Computer Modelling, **42**(9): 991-998.